The EUMETSAT Network of Satellite Application Facilities

OSI SAF
Ocean and Sea Ice

Algorithm theoretical basis document for the OSI SAF Sea and Sea Ice Surface Temperature L2 processing chain

OSI-205-a and OSI-205-b

Version 1.4

Gorm Dybkjær (DMI), Steinar Eastwood (MET), Anette Lauen Borg (MET), Jacob Høyer (DMI), Rasmus Tonboe (DMI)

19. February 2018

This page is intentionally left blank.

Document Change Record

Document Version	Date	Responsible	Description
v1.0	Feb. 2015	Gorm Dybkjær	For PCR
v1.1	April 2015	Gorm Dybkjær	Correction for RID
v1.2	March 2016	Steinar Eastwood	Inclusion of VIIRS and uncertainties
v1.3	June 2016	Steinar Eastwood	Correction for RIDs
V 1.4	Feb 2018	Steinar Eastwood	Added OSI-205-a

Table of Contents

1 Introduction

1.1 The EUMETSAT Ocean and Sea Ice SAF

For complementing its Central Facilities capability in Darmstadt and taking more benefit from specialized expertise in Member States, EUMETSAT created Satellite Application Facilities (SAFs), based on co-operation between several institutes and hosted by a National Meteorological Service. More on SAFs can be read from www.eumetsat.int.

The Ocean and Sea Ice Satellite Application Facility (OSI SAF) is producing on an operational basis a range of air-sea interface products, namely: wind, sea ice characteristics, Sea Surface Temperatures (SST), Surface Solar Irradiance (SSI) and Downward Longwave Irradiance (DLI). The sea ice products include sea ice concentration, the sea ice emissivity, sea ice edge, sea ice type and sea ice drift and sea ice surface temperature (from mid 2013).

The OSI SAF consortium is hosted by Météo-France. The sea ice processing is performed at the High Latitude processing facility (HL centre), operated jointly by the Norwegian and Danish Meteorological Institutes.

Note: The ownership and copyrights of the data set belong to EUMETSAT. The data is distributed freely, but EUMETSAT must be acknowledged when using the data. EUMETSAT's copyright credit must be shown by displaying the words "copyright (year) EUMETSAT" on each of the products used. User feedback to the OSI SAF project team is highly valued. The comments we get from our users is important argumentation when defining development activities and updates. We welcome anyone to use the data and provide feedback.

1.2 Scope

This Algorithm Theoretical Basis Document describes the computational steps for the integrated Sea and Ice surface temperature products, OSI-205-a and OSI-205-b. OSI-205-a/b will be implemented as part of the EUMETSAT OSI SAF programme. The document introduces and justifies the scientific assumptions and choices which are made. It does not deal with aspects of validation and user interface, as those issues will be dealt with in subsequent Validation Report (VR) and Product User Manual (PUM).

General information on the EUMETSAT OSI SAF is available from the OSI-SAF official web site: www.osi-saf.org.

1.3 Overview

Sea, ice and land surface temperatures largely control the exchange of energy between surface and atmosphere and sea ice models treat temperatures of snow/ice surfaces as a vital parameter for the development of sea ice in models. It has been estimated that a systematic surface temperature change of 1°C corresponds to an outgoing long wave radiation change of approximately 5 Wm-2. From a modeling point-of-view a systematic year round 5 W energy flux anomaly can be sufficient to change the sea ice regime from seasonal to perennial sea ice, or vice versa (Dybkjaer et al, 2012). This is crucial for sea ice modeling, because model analysis of sea ice surface temperatures may differ several degrees in average from satellite estimates (Dybkjaer et al., 2014).

There is a special awareness of the surface temperature in the Arctic because the

impact of global warming is estimated to be a factor of 2 higher than the average global warming. That is a consequence of the Arctic amplification, which is mainly caused by the albedo difference between the open water surface and ice/snow surfaces. A decreasing sea ice area results in increased surface absorption of incoming shortwave radiation, which leads to reduced new ice production throughout the freezing period. That is a self-reinforcing warming process, special for the Arctic. This effect is not evident in the Southern Ocean around Antarctica; however, for the reasons given above, it is crucial to monitor the sea and sea ice surface temperatures in both Antarctic and Arctic regions, with the primary purpose of assimilating the data into model systems and for model validation purposes.

Ocean, ice and atmosphere model development and validation is based on observation data. At very high latitudes, where the traditional observation network is sparse and observation records are few, satellite observations have since the 1970s been used to fill in the vast areas where in situ measurements do not exist.

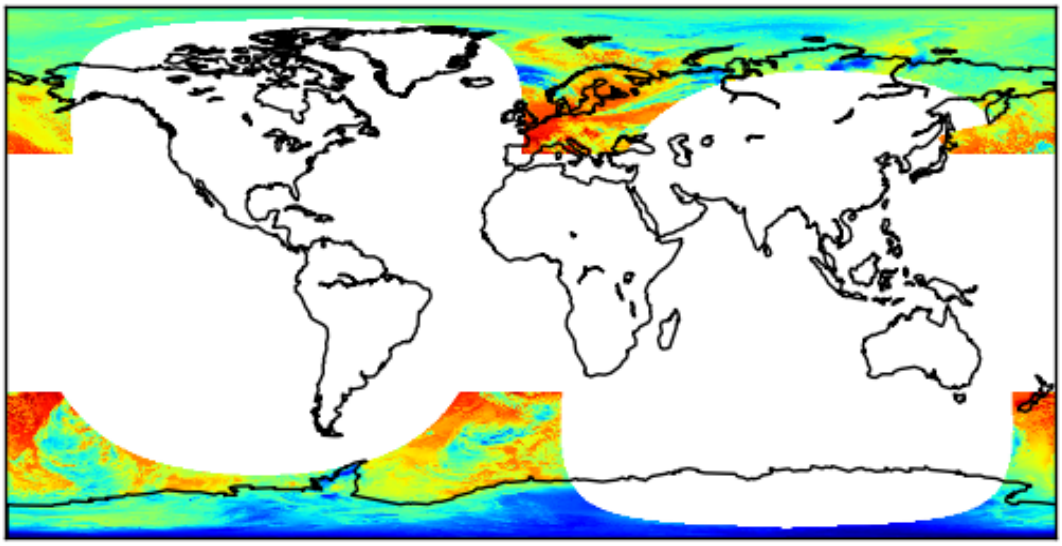

Figure 1: Coverage of a full orbit swath of Metop AVHRR level 2 brightness temperature data from the area of interest, i.e. above and below 50 North and 50 South, here projected onto a global map.

This ATBD describes the OSI SAF surface temperatures products (OSI-205-a/b) from thermal infrared satellite sensors, covering High Latitude Sea, Sea Ice and Ice Cap surface temperatures in the high latitude regions poleward of 50N/50S. The data production is dedicated to, and the algorithms are tuned to, atmospheric conditions at these high latitude regions, as illustrated in Figure 1. The target precision of the sea surface and sea ice surface temperature data are 1.0K and 4.0K, respectively, expressed as standard deviation of the difference with traditional buoy measurements (see PRD for details).

The input is thermal infrared data from the Advanced Very High Resolution Radiometer (AVHRR) on-board the EUMETSAT Metop satellites and from the Visible Infrared Imaging Radiometer Suite (VIIRS) on the Joint Polar Satellite System (JPSS) National Polar-orbiting Partnership (NPP) satellite. These data are a natural extension to one of the longest existing satellite records, namely data from the series of NOAA-AVHRR instruments. The OSI-205-a/b products are hence a possible extension of AVHRR based climate records, such as the AASTI data set (Dybkjær et al., 2014).

The OSI-205-a/b surface temperature data products are comparable to the MODIS IST/SST products that has been operating since 2002 (Hall et al. 2004 and 2006), and can be used together with the MODIS product for extended temporal coverage. The OSI-205-a/b products will also be used to build higher level products of time and space averaged surface temperatures, such as the OSI-203-b 12 hourly level 3 high latitude SST/IST product.

1.4 Glossary

AASTI - Arctic and Antarctic sea and sea ice Surface Temperatures from thermal Infrared satellite sensors, data set.
ATBD - Algorithm Theoretical Basis Document (This document)
AVHRR - Advanced Very High Resolution Radiometer
CAF - Central Application Facility, EUMETSAT
CDOP - Continuous Development and Operations Phase
DMI - Danish Meteorological Institute
EUMETSAT - European Organisation for the Exploitation of Meteorological Satellites
FOV - Field of View
GAC - Global Area Coverage
GDS - GHRSST Data Processing Specification
GHRSST - The Group for High-Resolution Sea Surface Temperature
IST - Sea Ice Surface Temperature
LEO - Low Earth Orbit
MET - Norwegian Meteorological Institute
Metop - EUMETSAT METeorological OPerational polar orbiting satellite
MIZT - The Marginal Ice Tone surface Temperature
MODIS - Moderate Resolution Imaging Spectroradiometer
NESDIS - National Environmental Satellite, Data, and Information Service, NOAA
NGDC - National Geophysical Data Center, NOAA
NOAA - National Oceanic and Atmospheric Administration
NWP - Numerical Weather Prediction
NWCSAF - Nowcasting - Satellite Application Facilities, at EUMETSAT
OSI SAF - Ocean and Sea Ice Satellite Application Facilities
OSTIA - The Operational Sea Surface Temperature and Sea Ice Analysis system
PUM - Product User Manual

SST - Sea Surface Temperature
VIIRS - Visible Infrared Imaging Radiometer Suite
VR - Validation Report

1.5 Applicable documents

A standard reference list is used, this is found at the end of the document.

2 Input Data

A number of input data are used to by OSI-205-a/b of which the primary data are brightness temperature (Tb) data from the Metop AVHRR and NPP VIIRS instruments. The surface temperature product is calculated from the Tb's and the associated view and sun angle information and a climatological SST temperature. In addition, data from the visible channels are used for the calculation of additional sea, ice and water probabilities. The Metop AVHRR and NPP VIIRS instruments provide a full orbit swath data set 14 times per day and thus provide approximately bi-hourly coverage of the polar regions. The Tb data, cloud mask and satellite-sun-earth geometry data are generated by Polar Platform System (PPS) cloud processing package, from the NWCSAF (NWCSAF, Dybbroe et al., 2005a+b).

The input data used by the surface temperature and cloud probability algorithms are provided by the PPS production software (NWCSAF); the data are Tb and reflectances, sun/satellite/earth geometrical information and the cloud mask data. Daily SST climatologies from the OSTIA system (Donlon, 2012) provided by the UK Met Office are also used by the daytime SST algorithm as a first SST guess (see below). All other data are ancillary fields of information that can be used as filters.

- *T37*, near IR Tb channel with centre wavelength at ~3.7 *μm* (channel 3b on AVHRR, M12 on VIIRS).
- *T8.6*, thermal IR Tb channel with centre wavelength at ~8.6 *μm* (channel M14 on VIIRS).
- *T11*, thermal IR Tb channel with centre wavelength at ~11 *μm* (channel 4 on AVHRR, M15 on VIIRS).
- *T12*, thermal IR Tb channel with centre wavelength at ~12 *μm* (channel 5 on AVHRR, M16 on VIIRS).
- *R06*, reflectance channel with centre wavelength at ~0.6μm (channel 1 on AVHRR, M4 on VIIRS).
- *R09*, reflectance channel with centre wavelength at ~0.9μm (channel 2 on AVHRR, M9 on VIIRS).
- *R16*, reflectance channel with centre wavelength at ~1.6μm (channel 3a on AVHRR, M10 on VIIRS).
- *satza*, sat-zenith angle.
- *sunza*, sun-zenith angle.
- *Cloud mask*, from PPS.
- *Tclim*, OSTIA daily climate value (OSTIA).

The PPS cloud mask consists of 5 categories:

- Unprocessed
- Cloud free
- Cloud contaminated
- Cloud filled
- Snow/Ice covered

Data pixels that are cloud free or snow/ice covered are considered cloud free, and

cloud filled and cloud contaminated pixels are considered cloudy. Each cloud category has a binary quality flag attached, i.e. the cloud mask quality is either high or low. A cloud mask quality value is labeled low quality when the value of a pixel in some feature is close to the threshold determining the category.

An overview of the processing chain and the data flow is illustrated in Figure 2.

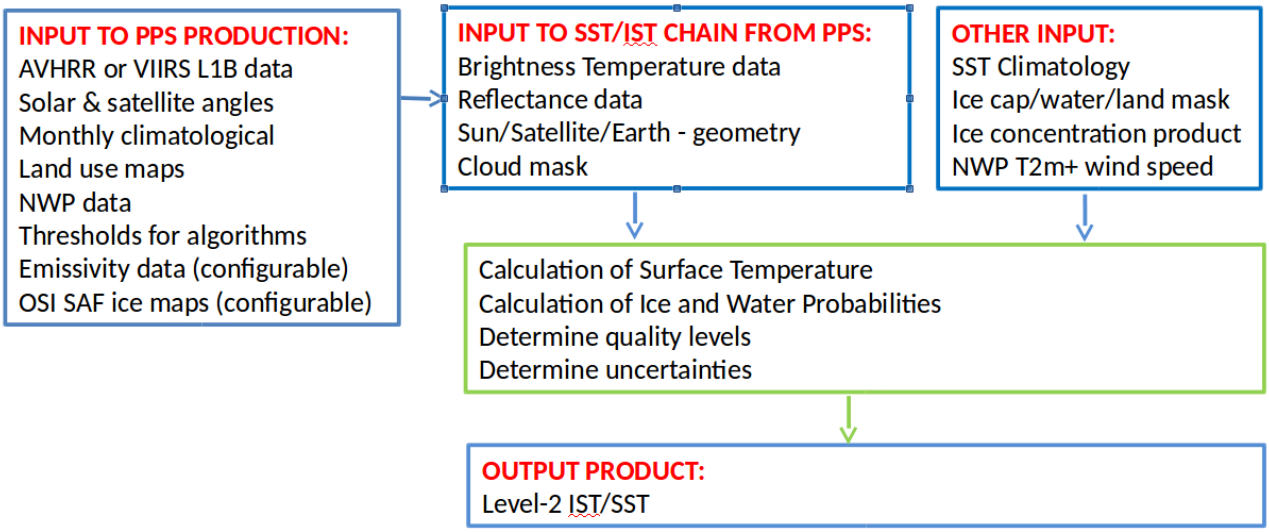

Figure 2: Overview of the Sea and Ice Surface Temperature (SST/IST) L2 processing chains (OSI-205-a/b). Blue rectangle illustrates input and data flow and the green rectangle illustrate the actual IST/SST production including calculation of ancillary fields.

3 Surface temperature algorithms

The OSI-205-a/b algorithm is in fact a suite of algorithms that are selected by different configurations of temperature and sun-zenith angle domains. The primary choice of algorithm lies in the distinction between sea and ice surfaces. This distinction is made from a simple brightness temperature threshold. This is an approach adapted from the integrated IST/SST algorithm CASSTA that was introduced by Vincent et al. (Vincent el al. 2008). The IST algorithm is subdivided into 3 temperature domains, each with its own algorithm, i.e. *cold*, *medium* and *warm* ice algorithms. The SST algorithm is made up by a *day*, a *night* and a *twilight* algorithm each triggered by sun-zenith angle. A temperature interval between the SST and IST algorithm domains is defined as the marginal ice zone. The marginal ice zone surface temperature (MIZT) algorithm is a scaled average of the IST and SST algorithms; hence, the MIZT is a mixed ice and water surface temperature.

3.1 Surface temperature decision tree

The algorithm selection and surface temperatures calculations are based on the three infrared channels, the solar-zenith angle and a first guess of SST, here represented by the daily climatologies from the OSTIA system (Donlon, 2012) provided by the UK Met Office.

The *IST* algorithm (equation 1) is a split window algorithm, working within three domains (Key et al., 1997). The algorithms coefficients are calculated within 3 *T11* temperature intervals (*cold*, *medium* and *warm*). The coefficients for IST algorithms are shown in Table 7 to Table 9, for Metop-A, Metop–B and NPP, respectively.

The *IST* temperature domains are:
- *ISTcold*, cold ice coefficients for *T11 < 240K*;
- *ISTmedium*, medium ice coefficients *for 240K ≤ T11 < 260K*
- *ISTwarm*, warm ice coefficients for *T11 ≥ 260K*;

$$IST = a + bT11 + c(\overline{T11 - T12}) + d(\overline{T11 - T12})steta, (Eq.1)$$

where $steta = \frac{1}{\cos(satza)} - 1$ and

$\overline{T11 - T12}$ is the average of all T11-T12 cloud free pixels in a 3x3 pixel box (see description below).

The sea surface temperature algorithms *SSTday* and *SSTnight* (Eq.2 and Eq.3, respectively) are, like the *IST* algorithm, determined for each domain, but for SST the domains are depending on the time of day:
- *SSTday*, day time algorithm for *sunza ≤ 90 degrees*. The day time algorithm formalism is a slightly modified version of the operational day time algorithm used in the OSI SAF SST product (OSISAF 2014) to deal with a slight bias for the North Atlantic area (Le Borgne et

al., 2014). For the case of *sunza* > 90 degrees (formaly night) and *T37* data are unavailable, the *SSTday* algorithm is enabled.

- *SSTnight*, night time algorithm for *sunza* ≥ *110 degrees*. The night time algorithm formalism is identical to the operational night time algorithm used in the OSI SAF Global SST product (OSISAF 2014)

The twilight algorithm is a scaled temperature of the SST*day* and SST*night* algorithms.

- *SSTtwilight*, twilight algorithm for *110 degree* ≥ *sunza* > *90 degree*. SSTtwilight is scaled linearly between *SSTday* and *SSTnight*, in accordance with the *sunza*, shown in equation 4 (OSI SAF 2014).

The *SST day* and *night* algorithm coefficients are shown in Table 7-Table 9, for Metop-A, Metop–B and NPP, respectively..

$$SSTday = (a + b\,steta)\,T11 + (c + d\,steta + e\,Tclim)(\overline{T11 - T12}) + f + g\,steta, (Eq.2)$$

$$SSTnight = (a + b\,steta)\,T37 + (c + d\,steta)(\overline{T11 - T12}) + e + f\,steta, (Eg.3)$$

$$SSTtwi\,light = 0.05(sunza - 90)\,SSTnight - 0.05(sunza - 110)\,SSTday, (Eq.4)$$

Finally, the surface temperature is also defined for a marginal ice zone, *MIZT*, as shown in equation 5. The *MIZT* is linearly scaled between *SST* and *IST* in the temperature interval of *268.95 K* ≤ *T11 < 270.95 K*.

$$MIZT = 0.5(T11 - 268.95)\,SST - 0.5(T11 - 270.95)\,IST, (Eq.5)$$

adapted from Vincent et al. (2008).

The atmospheric correction term (T11-T12) calculated for each pixel is the average value over all the cloud free pixels in the surrounding 3x3 pixel box. This average is used instead of the central pixel value to reduce the radiometric noise, and the atmospheric features (mainly the water vapour field) have much larger scale than the satellite pixel size.

For AVHRR we use the closest 3x3 neighbour pixels to define the average, even though the pixels are overlapping towards the end of the scan lines. For VIIRS, overlapping pixels at the end of the scan lines (off-nadir areas) are removed from the data set in a fixed «bow-tie» pattern and we take this into account when defining the 3x3 pixel box. The VIIRS sensor comprises 16 detectors in the along-track direction scanning across the track simultaneously. During the scan, the along-track direction grows as the angle moves away from nadir and the result is a significant scan-to-scan overlap. The removal of overlapping pixels at off-nadir in a bow-tie deletion pattern is repeated at a fixed rate, creating a visual artifact of "missing scan line segments" in raw images. To identify the 3x3 box of closest neighbours to a pixel, this fixed deletion pattern must be taken into account. If a pixel in a raw data file has a deleted neighbour in the along-track direction, the closest neighbour is in fact the next non-deleted pixel

in that direction.

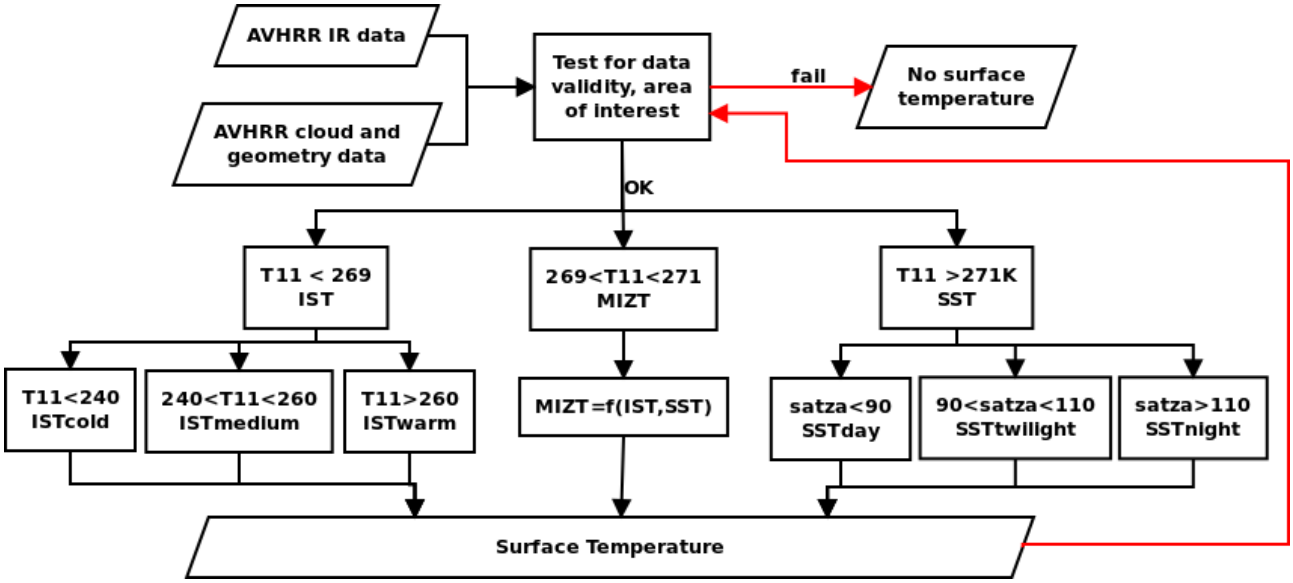

Figure 3: Surface temperature algorithm decision tree for OSI-205-a/b.

A schematic overview of the full algorithm decision tree is given in Figure 3. The input data are spectral AVHRR or VIIRS data and satellite-sun-earth geometry information. The red arrows indicate a double sanity check of the data. Firstly, a sanity check of the input brightness temperatures and a check for presence of a cloud mask value – if these checks fail -> no surface temperature will be calculated. This is indicated by the top red arrow. Secondly, a check of the calculated surface temperature – if the calculated value does not comply with the surface temperature test → the surface temperature will be rejected. The check of the surface temperature is indicated by bottom red arrow. In both cases the pixel will be flagged if it fails the tests. After validity check, the choice of algorithm is done based on temperature and sun elevation.

The data validity check is partly a check for area of interest, partly for data sanity and finally, a cloud check. The area of interest is north of 40N and south of 40S - in between these 2 parallels, the data is truncated. Further, a surface temperature is rejected if the data are flagged *missing* or *bad* and if (T11-T12) > 2.0 for T11 > 268.95 K. This is an indication of ice fog. Further, a surface temperature is rejected if the calculated surface temperature is less than *T11*, which is not possible, and if 150 K > Surface Temperature > 350K, which are unrealistic surface temperatures. In case of rejection, a flags is set in the output file. This is fully explained in the output NetCDF file.

Following this logic, a given pixel in the product is either rejected, with a flag value or a valid temperature value. In case of a valid temperature there is no guaranty that the value is ice or water. The temperature value can also represent cloud or land with no ice. The temperature value must therefore be checked for cloud, quality and a land

mask. All output data fields are described in the OSI-205-a/b Product User Manual.

3.2 Uncertainty estimation

For each pixel with a SST or IST retrieval, the random, locally systematic and large-scale systematic uncertainties are estimated. These uncertainty components represent errors that have distinct correlation properties. The uncertainty estimation steps are described below..

3.2.1 Random uncertainty

This is the random uncertainty due to errors unlikely to be correlated between pixels. It comprises geolocation precision uncertainty (U_{geo}) and noise equivalent differential temperature in temperature units ($U_{NEdT)}$), which are combined to make up the random component:

$$U_{rnd} = \sqrt{U_{geo}^2 + U_{NEdT}^2} \qquad \text{(Eq.6)}$$

The uncertainty in the temperature due to the satellite geolocation precision is found using the following equation taking into account the temperature difference between ice and water and the sea ice concentration. The empirical equation is derived from simulations of the imaging geometry.

$$U_{geo} = \left(T_{freeze} - \left(T_{ice} - T_{freeze} * \left(1 - N_{ice}\right)\right) / N_{ice}\right) * C_{geo} \quad , \qquad \text{(Eq.7)}$$

where N_{ice} is the ice concentration, T_{ice} is the temperature of the ice surface in Kelvin, T_{freeze} is the freezing temperature of sea water given as 271.35K and Cgeo is the geolocation coefficient, and empirical factor which is estimated using a satellite imaging simulator. It's magnitude depends on the geolocation uncertainty and the foot-print size. In the cases where the ice concentration is below 15% or above 85% U_{geo} is set to zero because of the limited inter pixel SST/IST variability over open water and near 100% ice. The maximum accepted value of U_{geo} is 2.

From the imaging simulator the geolocation coefficient for the Metop satellites has been found: $Cgeo_{metop} = 0.101.$ Tests with a satellite imaging simulator shows that Cgeo is approximately linear at sub-pixel resolution and it can be scaled to fit other satellites with comparable footprint size by taking into account their geolocation precision. As an example, assuming the pixel size of the metop satellites is approximately equal to that of the NPP satellite (1000 m vs 750 m) and their geolocation precision is 1000m and 100m respectively, the geolocation coefficient for NPP is:

C_{geo} (npp satellite) = 100m/1000m * C_{geo} (metop satellites)

The geolocation coefficient C_{geo} for each of the relevant satellites are listed in Table 1.

Satellite	Geo-location constant, Cgeo
Metop-A	0.101
Metop-B	0.101
NPP	0.0101

Table 1: The geolocation coefficient cgeo for each of the relevant satellites.

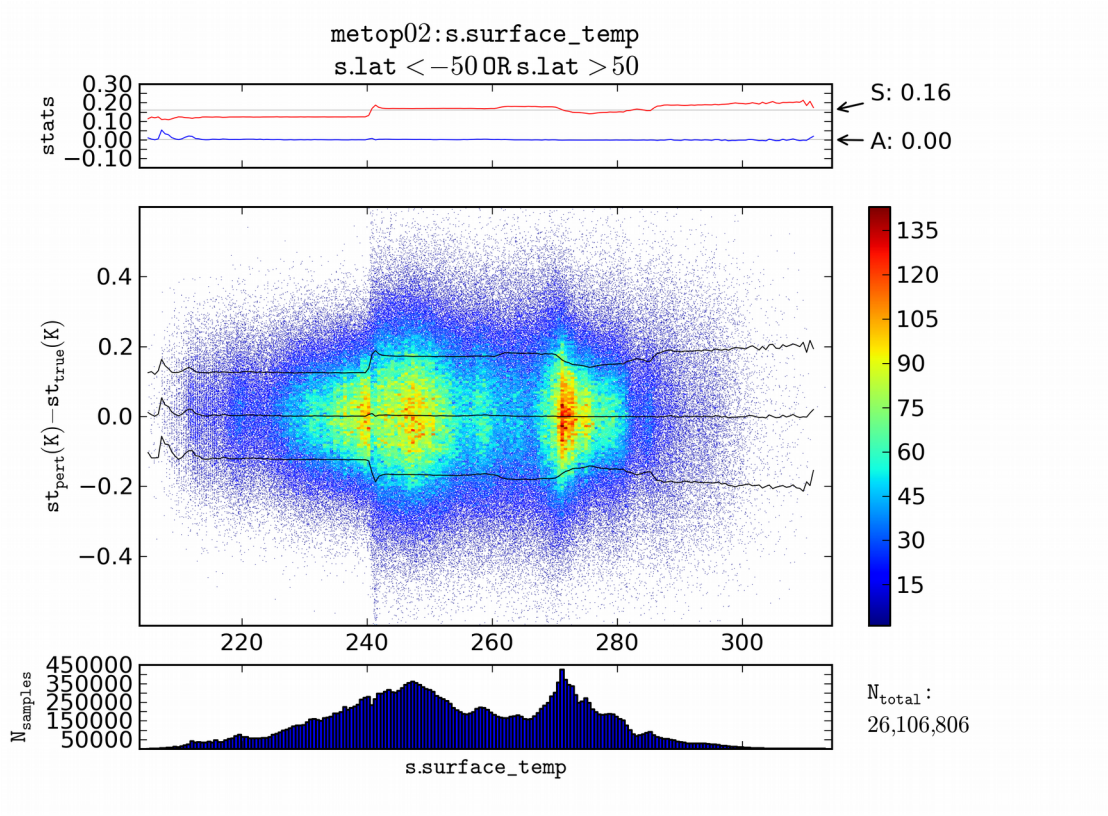

Figure 4: Difference between OSI-205-a/b surface temperature (ST) algorithm and corresponding ST calculated from perturbed Tb's. All Tb perturbations are within the instrument random noise level (NEdT value). Top plot is the STD and Bias (S and A) of ST-STperturbed as a function of ST. Middle plot shows the density plot of all ST-STperturbated values. For Metop—A data.

Noise equivalent differential temperature (NEdT) is radiometer specific and can be expected to depend on the scene temperature. In Table 2 the NEdT uncertainty component value is given for each relevant satellite and for each surface temperature algorithm (shown in the decision tree, Figure 3). The values are determined from propagating perturbed brightness temperatures through each algorithm for each sensor. The Tb's are perturbed randomly within the radiometer specific noise level. An example is shown in Figure 4. The NEdT are obtained from J. Mittaz (Mittaz, 2015 and Fiduceo, 2016). NEdT values are available per scan line from the AVHRR L1 data, but for this application the values from Mittaz (2015) were found well suited.

Satellite	*SST day*	*SST night*	*SST twilight*	IST warm	IST cold	IST mid	MIZT day	MIZT night	MIZT twilight
Metop-A	0.18205	0.10351	0.13713	0.17896	0.12403	0.16951	0.178734	0.14940	0.15818
Metop-B	0.18205	0.10351	0.13713	0.17896	0.12403	0.16951	0.178734	0.14940	0.15818
NPP	0.18205	0.10351	0.13713	0.17896	0.12403	0.16951	0.178734	0.14940	0.15818

Table 2: NEdT uncertainty component value is for Metop-A and Metop-B AVHRR sensors, for each surface temperature algorithm. For NPP VIIRS the same as Metop-A is currently being used.

3.2.2 Uncertainty likely to be correlated over synoptic scales

This component combines the uncertainty introduced by the emissivity variations due to the changes in satellite zenith angle and surface emissivity dependent uncertainty, and the residual of the fit for the regression-based retrieval algorithm:

$$U_{syn} = \sqrt{U_{emis}^2 + U_{fmt}^2} \qquad \text{(Eq.8)}$$

This uncertainty is simulated using a snow emissivity model described in Dozier and Warren (1982), measurements of snow density and grain size and the spectral response functions for the sensor.

As the satellite zenith angle changes the measured emissivity is affected. Uemis is given as a satellite zenith angle (sat_zen_angle) dependent equation:

$$\begin{aligned} Uemis &= 0.0001 * SatZenAngle + 0.0379, \text{for angles of } 0-44 \text{ degrees} \\ Uemis &= 0.0030 * SatZenAngle + 0.0912, \text{for angles of } 45-80 \text{ degrees} \end{aligned} \qquad \text{(Eq.9)}$$

The uncertainty component due to algorithm dependent uncertainty is given as the residual of the fit for the regression used to estimate the algorithm coefficients, as described in chapter 4. These residuals are given in Table 3 to Table 5 for all relevant satellites and algorithms.

Satellite	*SST day*	*SST night*	*SST twilight*	MIZT day	MIZT night	MIZT twilight	IST warm	IST cold	IST mid
Metop-A	0.314	0.277	0.2955	0.2255	0.207	0.21625	0.137	0.097	0.108
Metop-B	0.307	0.271	0.289	0.2255	0.2075	0.2165	0.144	0.102	0.121
NPP	0.338	0.263	0.3005	0.2555	0.218	0.23675	0.173	0.109	0.156

Table 3: Algorithm regression residuals that defines the algorithm uncertainty component, for Metop-A and Metop-B AVHRR, and NPP VIIRS. For Northern Hemisphere.

Satellite	*SST day*	*SST night*	*SST twilight*	MIZT day	MIZT night	MIZT twilight	IST warm	IST cold	IST mid
Metop-A	0.209	0.244	0.2265	0.147	0.1645	0.15575	0.085	0.093	0.123
Metop-B	0.208	0.245	0.2265	0.1465	0.165	0.15575	0.085	0.101	0.14
NPP	0.224	0.232	0.2303	0.167	0.173	0.171	0.107	0.105	0.178

Table 4: Algorithm regression residuals that defines the algorithm uncertainty component, for Metop-A and Metop-B AVHRR, and NPP VIIRS. For Southern Hemisphere.

Satellite	*SST day*	*SST night*	*SST twilight*	MIZT day	MIZT night	MIZT twilight	IST warm	IST cold	IST mid
Metop-A	-	-	-	-	-	-	0.178	0.199	0.26
Metop-B	-	-	-	-	-	-	0.182	0.203	0.278
NPP							0.224	0.225	0.376

Table 5: Algorithm regression residuals that defines the algorithm uncertainty component, for Metop-A and Metop-B AVHRR, and NPP VIIRS. For Ice Caps.

3.2.3 Uncertainty correlated over large/global scales

In Section 5.1 the quality levels of the SST and IST are described. Table 11 describes the levels from 5 (best quality) to 1 (bad data), with the addition of level 0 (no data). The quality levels describes effects that increase the uncertainties, but which are not part of the random and synoptic scale uncertainty components, such as proximity to clouds, high satellite zenith angle, twilight conditions and cold temperature estimate compared to climatology.

The large scale correlated uncertainty Uglob is the global residual uncertainties, in-cooperating the uncertainties represented by the quality levels. The Uglob values for each quality level have been set essentially by an expert judgment of the likely magnitude of the residual uncertainties. The expert judgement is based on experience from several calibration/validation activities against in situ temperature measurements, performed by the development team. Those activities include comparison of satellite IST measurements against multiple ground based radiometer data sets, air temperature data sets and data sets from Ice Mass-balance Buoy data sets, e.g Dybkjaer et al. 2012, DMI-TR 2011, Englyst et al. 2016 and Dybkjaer et al. 2014.
The Uglob values for each quality levels as shown in Table 6.

Quality level	Uglob
5	0
4	0.5
3	1
2	2
1	*Fillvalue*
0	*Fillvalue*

Table 6: Global scale uncertainties for the different quality levels.

4 Calculation of algorithm coefficients

There are basically two ways to calibrate the surface temperature algorithms used here: 1) To relate satellite measurements to in situ observations, and 2) to relate modeled surface temperatures with modeled top-of-atmosphere brightness temperatures, determined by a radiative transfer model (RTM).

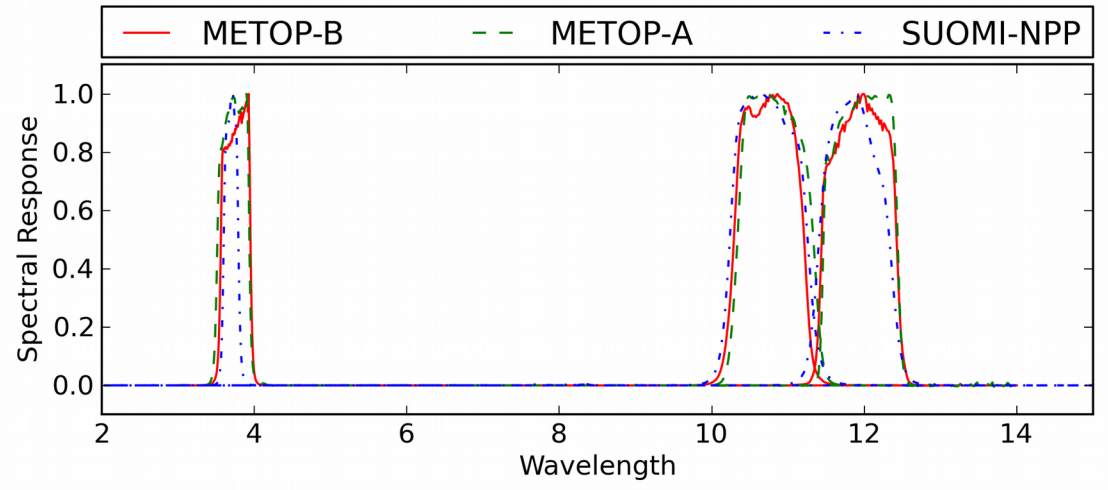

Figure 5: Spectral response functions for the 3.7, 11 and 12 um channels on Metop-A, Metop-B and Suomi-NPP.

Calculations of algorithm coefficients for both the IST and SST algorithms are carried out using the RTM-approach. All algorithm coefficients in the following are valid for temperatures in Kelvin. Algorithm coefficients are determined with individual AVHRR channel response functions (Figure 5) and angular dependent emissivity (Figure 6).

4.1 SST algorithm coefficients

Coefficients for the SST algorithms were generated using a simulated brightness temperature (Tb) data-set in turn generated from a data-set containing 31,673 Arctic profiles (Francois et al., 2002). The simulated Tb's were generated from RTTOV11.1 (Hocking et al, 2014) using 10 different satellite zenith angles (0.0, 36.87, 48.19, 55.15, 60, 63.61, 66.42, 68.68, 70.53, 72.08). Coefficients for each algorithm were determined using least squares regression. The coefficients for SSTday and SSTnight algorithms are shown in Table 7, Table 8 and Table 9, for Metop-A, Metop-B and NPP, respectively.

Metop-A	a	b	C	d	e	f	g
SSTday	1.03039	0.01749	-0.29966	0.25514	0.00629	-8.13237	-3.7373
SSTnight	1.01937	0.03637	1.1998	0.0582	-4.45263	-8.87747	-
ISTcold	-3.21614	1.01371	0.86601	0.03649	-	-	-
ISTmedium	-3.20022	1.01295	1.44255	0.0237	-	-	-
ISTwarm	-3.87652	1.01525	1.46076	0.31115	-	-	-

Table 7: SST and IST algorithm coefficients for Metop-A AVHRR (coefficients are defined in equation 1-3).

Metop-B	a	b	C	d	e	f	g
SSTday	1.03337	0.01860	0.32580	0.26096	0.00383	-8.87140	-3.95122
SSTnight	1.01938	0.03654	1.17970	0.06157	-4.38415	-8.85729	-
ISTcold	-3.29453	1.01404	0.74924	0.01508	-	-	-
ISTmedium	-4.01702	1.01615	1.41726	-0.03038	-	-	-
ISTwarm	-4.61195	1.01815	1.37783	0.30656	-	-	-

Table 8: SST and IST algorithm coefficients for Metop-B AVHRR (coefficients are defined in equation 1-3).

NPP VIIRS	a	b	C	d	e	f	g
SSTday	1.03039	0.01749	-0.29966	0.25514	0.00629	-8.13237	-3.7373
SSTnight	1.01937	0.03637	1.1998	0.0582	-4.45263	-8.87747	-
ISTcold	-3.21614	1.01371	0.86601	0.03649	-	-	-
ISTmedium	-3.20022	1.01295	1.44255	0.0237	-	-	-
ISTwarm	-3.87652	1.01525	1.46076	0.31115	-	-	-

Table 9: SST and IST algorithm coefficients for NPP VIIRS (coefficients are defined in equation 1-3).

4.2 IST algorithm coefficients

Like tuning of the SST algorithms, calculation of the IST algorithm coefficients is carried out using modeled surface and TOA brightness temperatures. The basis for the algorithm coefficients is an Arctic profile database covering one year (2011) of ERA Interim atmospheric data (ERAint, 2014-09).

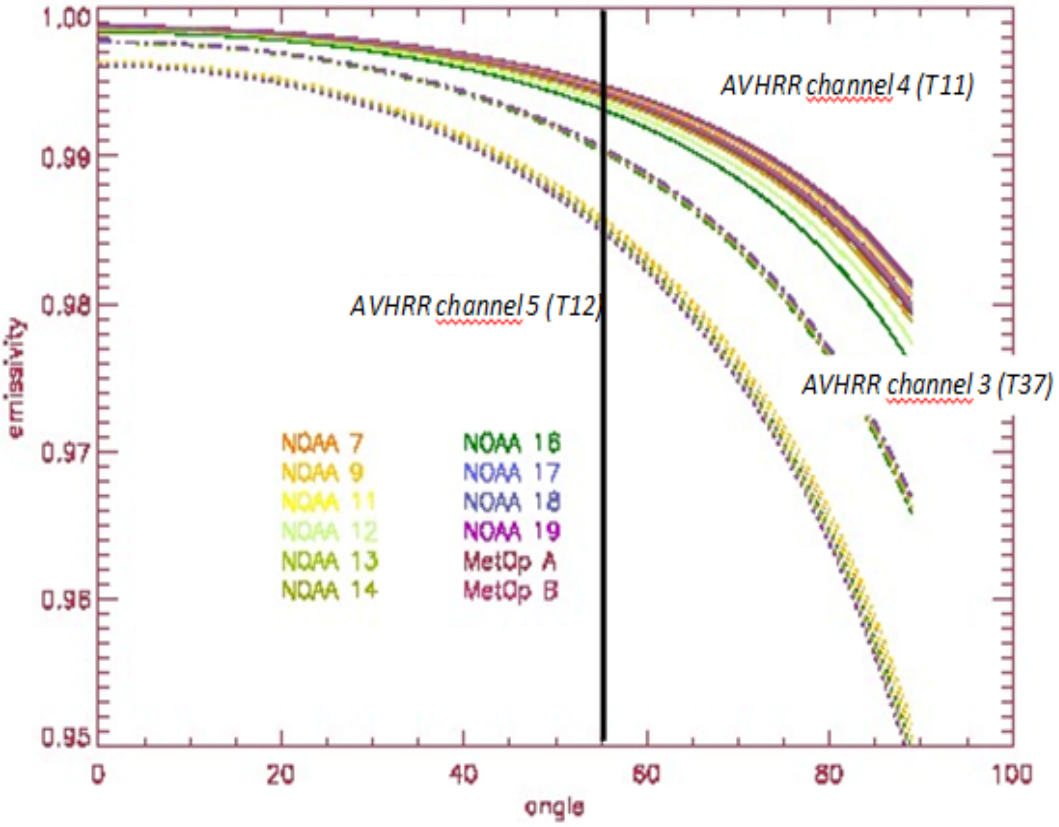

Figure 6: The snow emissivity as a function of viewing angle for all operational AVHRR instruments since 1982. The top group of emissivity curves correspond to the AVHRR channel 4 emissivities (T11), the middle group correspond to the AVHRR channel 3 emissivities (T3.7) and the bottom group of emissivity curves correspond to the AVHRR channel 5 emissivities (T12). The vertical line at 55 degree scan angle indicates the upper scan angle limit of data used for this application.

The initial profile database has 8,695 profiles, see Figure 7. Profiles were picked from a sample of 960 locations each day of the year, at times 0, 6, 12 and 18 UTC. Each profile complies with a land-ratio of zero, surface temperatures less than 272K, a cloud cover of less than 10% and ice concentration greater than 90%. Simulated TOA brightness temperatures associated with the ERA-interim surface temperatures for over 10 different satellite zenith angles (0.0, 36.87, 48.19, 55.15, 60, 63.61, 66.42, 68.68, 70.53, 72.08), were generated using RTTOV11.1 (Hocking et al, 2014). Ultimately, the simulated IST tuning data set consisted of 86,950 data points.

RTTOV11 includes a model for calculating sea surface emissivities but does not include a model for land or sea ice. Instead, as a default, RTTOV will use hardcoded values of 0.98 (land) and 0.99 (sea ice), respectively, if the user indicates that RTTOV should 'calculate' the surface emissivity.

To describe the snow emissivity as a function of the incidence angle we have used a snow emission model with a typical snow type as input. The model used here is described in Dozier and Warren (1982) and it uses snow surface density at 300 kg/m3 and snow grain size at 100 microns. The simulated spectral emissivity is folded with the spectral response function for each of the channels *T37*, *T11* and *T12* and for a wide range of AVHRR instruments and the VIIRS instrument, and used as the angle dependent snow surface emissivity in the RTTOV simulations for estimating the IST algorithm coefficients.

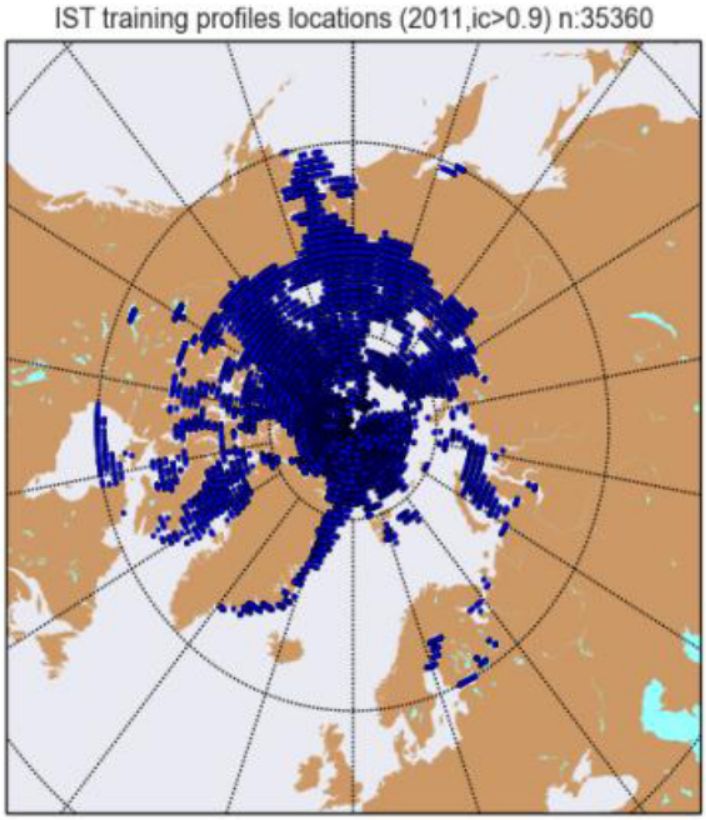

Figure 7: Atmospheric profile positions for calculation of IST algorithm coefficients.

The calculated and applied angular dependent emissivities are plotted in Figure 6, for each channel and for a whole series of AVHRR sensors (VIIRS not included in this plot).

The full coefficient tables for the *ISTcold*, *ISTmedium* and *ISTwarm* algorithms are shown in Table 7-Table 9. The IST algorithm coefficients are defined in Eq.1.

There is a documented warm bias in ERA INTERIM surface temperature (Lupkes et al. 2010 and Jakobson et al. 2012). It is not expected that this warm bias will have an effect on algorithm coefficients. The ERA INTERIM data set provides a wide variety of realistic data pairs of surface temperatures and atmospheric water content and not

necessarily correct surface temperatures. The atmospheric transfer model, RTTOV, is responsible for calculating the corresponding Top Of Atmosphere (TOA) radiation from which the coefficients are determined.

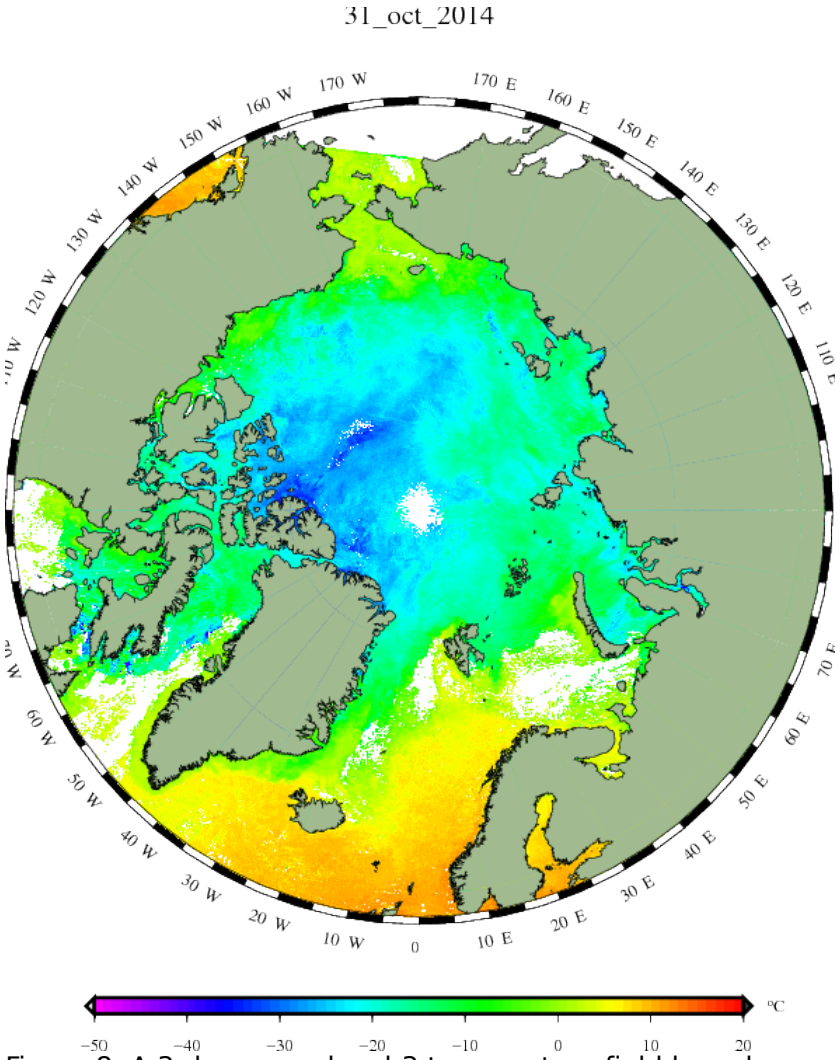

Figure 8: A 3-day mean level-3 temperature field based on OSI-205-b. This plot is included to illustrate the integrated IST, MIZT and SST product. OSI-205-a/b is only produced in level-2.

5 Calculation and determination of ancillary fields

5.1 Quality levels

Quality levels are designed to help users to filter data that are not sufficiently good for their purpose. We adopt the recommendation of the GHRSST formalized through the GDS v2 document. For infrared derived SST (and also IST here, which is not yet a GDS standard) six quality levels are defined. 0: unprocessed; 1: bad/cloudy, 2: worst, 3: low, 4 acceptable, 5 excellent. Quality level assessment is based on the degree of compliance to quality conditions. Degree of compliance is based on error impact classes minor and major. The conditions the IST and SST values are tested against are shown in Table 10. The applied conditions are selected from empirical validation experience as being conditions that have significant impact on the overall precision of the remaining data.

	Clima-tology	**CloudMask (cm)**	**cm-quality**	**Cloud-box (3x3)**	**Scan-angle**	**Sunzen-angle**
IST-test	NA	Not cloudy	High	All free	<60	>80
IST: No-comply penalty		Major	Minor	Minor	Minor	Minor
SST-test	diff<10	Not cloudy	High	All free	<60	<80 or >95
SST: No-comply penalty	Minor	Major	Minor	Minor	Minor	Minor

Table 10: IST and SST test criteria to comply with – for pixel-wise quality assessment. The notation 'No-comply penalty' indicate, the penalty given if a given pixel does not comply to the test – either minor or major. The tests are: diff<10: the difference between a given surface temperature and the corresponding value from ECMWF surface temperature. The absolute difference must be less than 10K. Not-cloudy: a pixel must be cloud free or ice contaminated. Cm-quality high: The cloud mask quality indicator must be of high-quality (an information from the PPS data stream). Cloud-box 3x3: all 8 adjacent pixels must be cloud free or ice contaminated. Scan-angle <60: Scan angle (view angle) must be less than 60 degrees. Sunzen-angle >80 / <80 or >95: Sun-zenith angle must be greater than 80 degrees / less than 80 or greater the 95 degrees.

QL 5, best	Comply to all criteria
QL 4, acceptable	Fail 1 minor criterion
QL 3, low	Fail 2 minor criteria
QL 2, worst	Fail 3 or more minor criteria
QL 1, bad	Fail 1 major or more criteria, or flagged, i.e. T outside 150-350K
QL 0, no data	Everything else

Table 11: Pixel-wise quality estimate, based on degree of failed compliance to criteria in Table 10.

5.2 Land/Sea/Greenland/Antarctic-ice-sheet mask

Land mask from NOAA NESDIS NGDC global relief maps (NOAAngdc, 2014-09). From 'ice_surface' and 'bedrock' ETOPO1 data sets, a land, sea and land ice mask is produced. The procedure below is used. Thresholds of 10m and -5m are chosen to minimize noise in the relief maps.

a) ICE CAP: 'ice_surface' - 'bedrock' > 10 m
b) SEA (including sea ice areas): 'ice_surface' - 'bedrock' <= -5 m
c) LAND: Where NO ICE CAP and NO SEA.

This is an add-on data set for stratification of land, sea and ice caps (see 'output data'). It is not used for surface temperatures calculations.

5.3 Probability of water, ice and cloud

Cloud and ice masking is inherently difficult over cold snow and ice surfaces, and in particular at night and at low sun elevations which are a characteristic of the high latitudes. But masking out clouds is crucial for the OSI SAF SST/IST retrieval.

Therefore, an additional step is applied in the processing to detect clouds and ice not discovered by the PPS cloud mask. This step includes calculation of the probability of a pixel being cloud free water, cloud free ice/snow, or cloudy. It uses a naïve Bayesian approach based on probability density functions for water, ice and clouds. The probability of water and ice are produced and added to the output data to provide additional filtering means for the user, to minimize further the risk of using cloud contaminated surface temperature values.
The probabilities of water, ice and cloud given two features (x.yx) from one set of observed satellite channel values are defined as follows:

$$ProbIce(x,y) = prob(featX|ice,x) * prob(featY|ice,y) / psum(x,y)$$
$$ProbWater(x,y) = prob(featX|water,x) * prob(featY|water,y) / psum(x,y)$$
$$ProbCloud(x,y) = prob(featX|cloud,x) * prob(featY|cloud,y) / psum(x,y)$$

, Eq.10

$$where\ psum = prob(featX|ice,x) * prob(featY|ice,y) + prob(featX|water,x) * prob(featY|water,y) + prob(featX|cloud,x) * prob(featY|cloud,y)$$

x, y *are the observed values of features featX , featY , respectivly .*

This equation is for the case of two features being used. The equation can also be extended to more features or simplified to one feature. A feature is in this context a single satellite channel value (reflectance or brightness temperature), a combination of two (or more) channel values or a derived value such as local spatial variance of a channel value.

5.3.1 Daytime probabilistic classifier

For the daytime probabilistic classifier, the following three features have been selected, based on their capacity to separate between different ice, water and clouds :

- r0.9/r0.6 (mainly separate water from ice and clouds)
- r1.6/r0.6 (mainly separate ice and water from clouds)
- r0.6 (additional separation of water from ice and clouds)

The probabilities of ice, water and cloud given a set of three observed features (r0.9/r0.6, r1.6/r0.6, r0.6) are calculated from the probabilities of these three features give ice, water and clouds, or by the probability density functions (PDFs). Such PDFs have been defined for these three features and the three classes ice, water and clouds. The PDFs have been defined using selected training data, with satellite data and a prior classification of the three classes from the PPS cloud mask. Simulated satellite data from a radiative transfer model could also have been used, but a prior classification from PPS was found most appropriate for our purpose.

For the daytime classifier the PDFs are 2 dimensional, depending on the solar zenith angle, and they have been estimated for several instruments, including AVHRR on Metop-A and Metop-B, and VIIRS on NPP. The PDFs are given as tables of mean (M) and standard deviations (S) for normal distributions for each satellite zenith angle. From these PDFs, the probability for a feature X given a class can be calculated for all range of observed values x in this feature, by the following equation:

$$prob(featX|class,x) = NormalDist(x, M(featX,class), S(featX,class)),$$
$$where$$
$$NormalDist(x,M,S) = (1.0(S*\sqrt{(2.0*PI)})) * \exp((x-M)^2/(2.0*S^2)) \quad \text{(Eq.11)}$$

Eq.11 is then solved using Eq.10 to find the probabilities for each class, given the

observed values of the features. More details about the PDFs and the procedures for calculating these probabilities are fully explained in Killie et al. (2011) and a comparison with the PPS cloud mask is shown in Dybbroe et al. (2014). Examples of the PDFs and their dependence on solar zenith angle are shown in Figure 9. Examples of probability estimates for water, ice and clouds for a Metop-A AVHRR swath are shown in Figure 10.

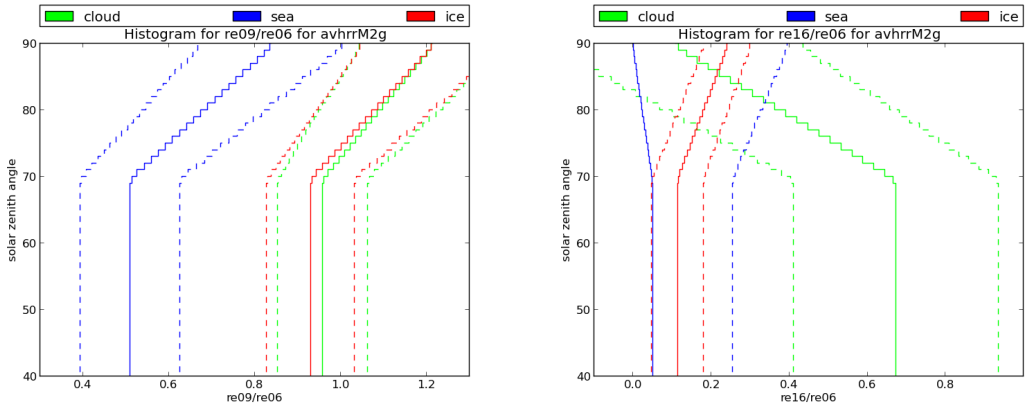

Figure 9: Mean (solid lines) +/- one standard deviations (dashed lines) of the normal distributions defining the PDFs for cloud (green), water (blue) and ice (red) for r0.9/r0.6 (left) and r1.6/r0.6, as function of solar zenith angle. For Metop-A.

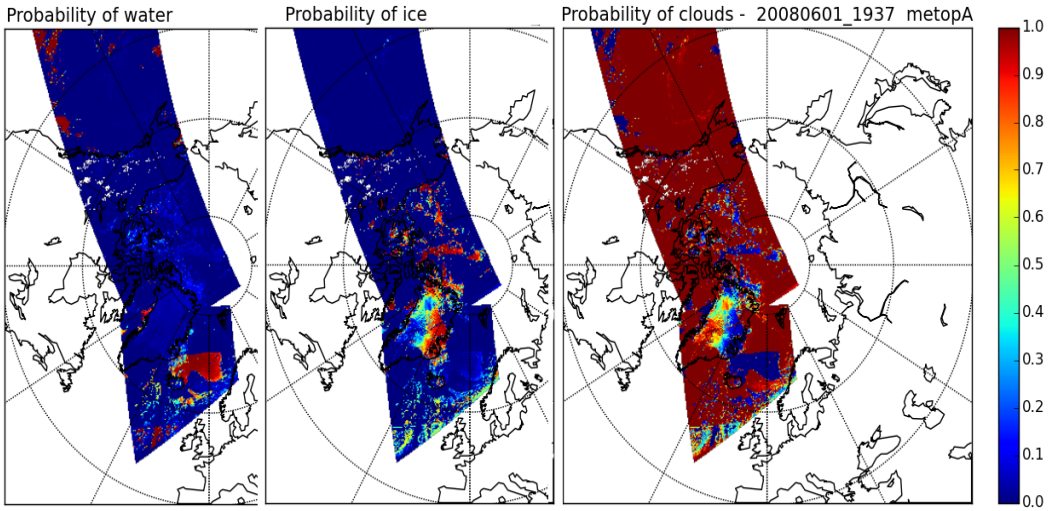

Figure 10: Example of fields for probability of water, ice and clouds from a METOP-A orbit from 2008.06.01 1937 UTC.

5.3.2 Night time probabilistic classifier

For the night time probabilistic classifier, a similar approach is used as for the daytime classifier. The main difference is that two 4-D variable histograms are used to calculate the probabilities for the observations given ice, water and clouds in Eq.10, instead of the set of 2-D PDFs used at daytime. The use of multidimensional histograms is especially useful at night time, since the available IR observations tend to be more correlated than the different visible channels at daytime.
The 4-D variable histograms use the following features:

1. T11-T12, T3.7-T12, T8.6-T11, sat-zenith-angle
2. Tsurf, T11-Tsurf, T11-T12, T3.7-T12

For Tsurface the closest in time surface temperature from ECMWF NWP model is used.
These multidimensional histograms have been defined by using 2 years of PPS cloud mask products and counting the all occurrences of each class (ice, water, cloud) in bins of the features defining the histogram. The histogram is then normalized for each class separately, by dividing each bin with the maximum number of counts. This turns the histogram into a PDF that can be used directly in Eq.10, without using Eq.11.
These histogram-based PDFs are defined in NetCDF files with 4-D fields for each of the three classes.

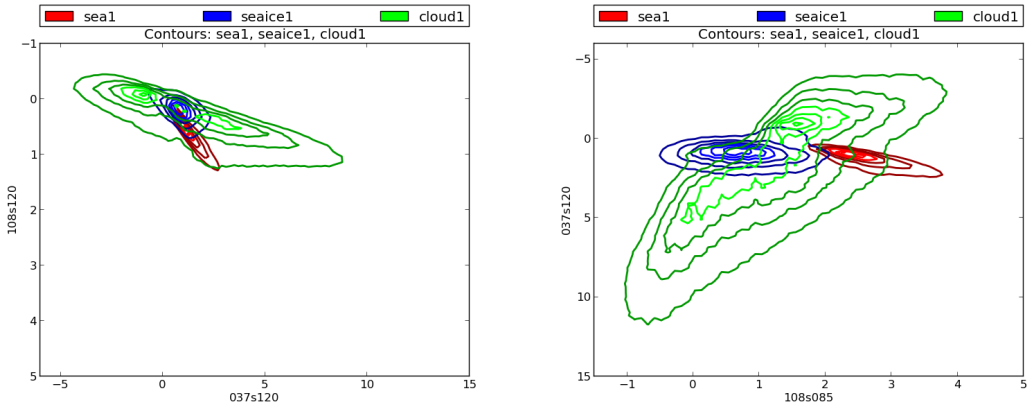

Figure 11: Contour plot for two set of features (left: 3.7-12.0um vs 10.8-12.0um, right: 10.8-8.5um vs 3.7-12.0um) which are part of the 4D PDF for VIIRS nighttime ice-water-cloud masking. In red: water, blue: ice, green: cloud.

6 Validation and technical aspects

6.1 Algorithm validation

The validation plan for this satellite based Sea and Ice surface temperature product is divided into a routine validation procedure and a validation procedure for opportunities. The former is a continuous validation procedure using traditional buoy and ship measurements from the GTS data stream, including the uncertainties mentioned above. Validation of opportunity is an additional product validation procedure against ship borne radiometer measurements or other more accurate surface temperature measurements than traditional buoy measurements.

The aim of a continuous control is to make available on a near real time basis (immediately after the production) relevant information to quickly detect a problem in the functioning of the chain and that there is no deviation in time. It consists in a series of maps and graphics that inform about the successful development of such and such step of the processing chain. The control is performed outside the operational environment and it is not visible to external users.

The continuous validation and monitoring plan monitors error and bias and the ratio of cloud free pixels. The validation plan is similar to what was done for the previous and present operational global OSI SAF LEO SST processing chain; see Le Borgne et al. (2008) and Saux Picart (2014).

In-situ observations of ice surface temperatures in Arctic regions are typically measured by buoys on the sea ice. Such measurements are often dubious because the instrument can be buried under snow or sticking up in the air and thus measuring either internal snowpack temperatures or air temperatures. Snow, snow skin and air temperatures can in fact be several degrees apart and validation of the skin temperatures measured from satellite is therefore complicated. For this reason, the validation requirements for the OSI SAF IST products have been split in two, one set of requirements for validation based on in situ IR radiometers and one set for validation based on in situ temperature buoys. The requirements for IST radiometer validation are more precise and accurate than those for buoy validation, since radiometers provide a more representative observation of the temperature that the IST product delivers. The IST requirements are partly based on Stammer et al. (2007) and the validation requirements are listed in Table 12. Validation and other product requirements are described in the Product Requirement Document (PRD, 2017).

	Threshold accuracy		Target accuracy		Optimal accuracy	
	Std.dev	Bias	Std.dev	Bias	Std.dev	Bias
SST	1.5 C	1.5 C	1.0 C	0.7 C	0.3 C	0.1 C
IST - radiometer	3.0 C	2.5 C	2.0 C	1.5 C	0.8 C	0.5 C
IST - buoys	4.0 C	4.5 C	3.0 C	3.5 C	1.0 C	0.8 C

Table 12: Monthly accuracy requirements for SST and IST for OSI-205-a/b. IST requirements split between validation against radiometers and buoys.

6.2 Error estimates

Sensor Specific Error Estimates (SSES) will be provided for each pixel, based on the GHRSST common principles (GHRSST, 2012). The SSES are observational error estimates provided at pixel level as a bias and standard deviation. These SSES statistics will be based on the validation exercise to be performed during the implementation of the processing software, using one full year of data.

6.3 Exception handling

1. In the case of pixel or scan lines of missing data, no SST or IST values will be calculated or estimated.
2. In the case of PPS cloud mask failure, either on pixel, scan line or complete swath file basis, no SST or IST values will be calculated for that pixel, scan line or swath file.
3. In the case of the expected sea ice product file is missing, an older sea ice product file will be used.

6.4 Assumptions and Limitations

1. There is no additional geolocation correction procedures applied to the AVHRR and VIIRS data; it is assumed that the geolocation quality is sufficient.
2. There may be periods where the statistical basis for IST validation is limited, due to periodically poor coverage of in situ observations.

6.5 Computer and programming considerations

No re-gridding or averaging is performed to the OSI-205-a/b product. The output projection and area is identical to the 3-minute input segment. The OSI-205-a/b processing is written in C programming language using common C-libraries and special OSI SAF libraries from the OSI SAF SVN repository. The final OSI-205-a/b product will occupy approximately 2.4 GB of disk space for global AVHRR and 2.2 Gb for EARS retransmission VIIRS data , daily, in netCDF 4 compressed data files.

6.6 NetCDF product header

Below is given a draft example of the NetCDF product header.

```
netcdf sst-ist_l2_npp_viirs_20160621_0806_24091 {
dimensions:
        time = 1 ;
        ni = 3200 ;
        nj = 8448 ;
variables:
        double time(time) ;
                time:units = "seconds since 1978-01-01 00:00:00" ;
                time:long_name = "reference time of ST fields" ;
                time:standard_name = "time" ;
                time:calendar = "Gregorian" ;
        float lat(time, nj, ni) ;
                lat:units = "degrees_north" ;
                lat:long_name = "latitude coordinate" ;
                lat:standard_name = "latitude" ;
                lat:valid_min = -90.f ;
                lat:valid_max = 90.f ;
        float lon(time, nj, ni) ;
                lon:units = "degrees_east" ;
                lon:long_name = "longitude coordinate" ;
                lon:standard_name = "longitude" ;
                lon:valid_min = -180.f ;
                lon:valid_max = 180.f ;
        short land_mask(time, nj, ni) ;
                land_mask:units = "" ;
                land_mask:long_name = "Land" ;
                land_mask:standard_name = "Land" ;
                land_mask:coordinates = "lon lat" ;
                land_mask:valid_min = 0.f ;
                land_mask:valid_max = 1000.f ;
        byte sea_ice_fraction(time, nj, ni) ;
                sea_ice_fraction:units = "1" ;
                sea_ice_fraction:long_name = "sea_ice_concentration" ;
                sea_ice_fraction:standard_name = "sea_ice_area_fraction" ;
                sea_ice_fraction:coordinates = "lon lat" ;
                sea_ice_fraction:scale_factor = 0.01f ;
                sea_ice_fraction:add_offset = 0.f ;
                sea_ice_fraction:time_offset = -4612s ;
                sea_ice_fraction:valid_min = 0b ;
                sea_ice_fraction:valid_max = 100b ;
                sea_ice_fraction:_FillValue = -100b ;
                sea_ice_fraction:source = "OSI SAF reprocessed sea ice concentration product (OSI-409) v1.1" ;
```

sea_ice_fraction:file_quality_level = 3 ;

short surface_temperature(time, nj, ni) ;

surface_temperature:units = "K" ;

surface_temperature:long_name = "sea and sea ice temperature" ;

surface_temperature:standard_name = "surface_temperature" ;

surface_temperature:coordinates = "lon lat" ;

surface_temperature:comment = "Temperature of the skin of the ocean and ice" ;

surface_temperature:scale_factor = 0.01f ;

surface_temperature:add_offset = 0.f ;

surface_temperature:valid_min = 15000s ;

surface_temperature:valid_max = 32315s ;

surface_temperature:_FillValue = -32768s ;

short sea_surface_temperature(time, nj, ni) ;

sea_surface_temperature:units = "K" ;

sea_surface_temperature:long_name = "sea surface subskin temperature, 1 to 1.5 millimetres" ;

sea_surface_temperature:standard_name = "sea_surface_subskin_temperature" ;

sea_surface_temperature:coordinates = "lon lat" ;

sea_surface_temperature:depth = "1 to 1.5 millimetres" ;

sea_surface_temperature:scale_factor = 0.01f ;

sea_surface_temperature:add_offset = 0.f ;

sea_surface_temperature:valid_min = 27115s ;

sea_surface_temperature:valid_max = 32315s ;

sea_surface_temperature:_FillValue = -32768s ;

short sst_dtime(time, nj, ni) ;

sst_dtime:units = "seconds" ;

sst_dtime:long_name = "time difference from reference time" ;

sst_dtime:standard_name = "time" ;

sst_dtime:coordinates = "lon lat" ;

sst_dtime:scale_factor = 1.818182f ;

sst_dtime:add_offset = 0.f ;

sst_dtime:valid_min = -32768s ;

sst_dtime:valid_max = -32768s ;

sst_dtime:_FillValue = -32768s ;

sst_dtime:comment = "reference time plus st_dtime gives seconds after 1978-01-01 00:00:00 UTC" ;

short l2p_flags(time, nj, ni) ;

l2p_flags:long_name = "L2P flags" ;

l2p_flags:comment = "These flags are important to properly use the data. The land-water-ice mask is produced from the NOAA NESDIS NGDC GLOBAL RELIEF MAPS, ETOPO1 Ice Surface and ETOPO1 Bedrock (http://www.ngdc.noaa.gov/mgg/global/global.html). Cloud mask data is from the PPS cloud mask. " ;

l2p_flags:coordinates = "lon lat" ;

l2p_flags:flag_meanings = "microwave land ice lake river reserved_for_future_use ice-cap water land cloudmask_quality_high cloudmask_not_processed cloud_free cloud_contaminated cloud_filled snow_ice_contaminated undefined" ;

l2p_flags:valid_min = 0s ;

l2p_flags:valid_max = 32767s ;

l2p_flags:flag_masks = "1s, 2s, 4s, 8s, 16s, 32s, 64s, 128s, 256s, 512s, 1024s, 2048s, 4096s, 8192s, 16384s, 32768s" ;

l2p_flags:_FillValue = -32768s ;

short processing_flags(time, nj, ni) ;

processing_flags:_FillValue = -32768s ;

processing_flags:long_name = "processing and algorithm flags" ;

processing_flags:coordinates = "lon lat" ;

processing_flags:valid_min = 0s ;

processing_flags:valid_max = 4096s ;

processing_flags:flag_meanings = "no_algorithm sst_day sst_night sst_twilight istwarm istmid istcold miszt_day miszt_night mizt_twilight Ts<T11 for268.95<=T11<270.95_T11-T12>2 forT11>=270.95_T11-T12>2 " ;

processing_flags:comment = "These flags are important to properly use the data." ;

processing_flags:flag_masks = "1s, 2s, 4s, 8s, 16s, 32s, 64s, 128s, 256s, 512s, 1024s, 2048s, 4096s" ;

byte quality_level(time, nj, ni) ;

quality_level:long_name = "quality level of st pixel" ;

quality_level:comment = "These are the overall quality indicators and are used for all SIST and SST values" ;

quality_level:coordinates = "lon lat" ;

quality_level:flag_meanings = "no_data bad_data worst_quality low_quality acceptable_quality best_quality" ;

quality_level:flag_values = "0b, 1b, 2b, 3b, 4b, 5b" ;

quality_level:valid_min = 0s ;

quality_level:valid_max = 5s ;

quality_level:_FillValue = -100b ;

byte sses_standard_deviation(time, nj, ni) ;

sses_standard_deviation:long_name = "SSES standard deviation" ;

sses_standard_deviation:units = "K" ;

sses_standard_deviation:coordinates = "lon lat" ;

sses_standard_deviation:valid_min = -127s ;

sses_standard_deviation:valid_max = 127s ;

sses_standard_deviation:_FillValue = -100b ;

byte sses_bias(time, nj, ni) ;

sses_bias:long_name = "SSES bias estimate" ;

sses_bias:units = "K" ;

sses_bias:coordinates = "lon lat" ;

sses_bias:valid_min = -127s ;

sses_bias:valid_max = 127s ;

sses_bias:_FillValue = -100b ;

byte probability_of_water(time, nj, ni) ;

probability_of_water:long_name = "probability of water" ;

probability_of_water:units = "percent" ;

probability_of_water:comment = "Sum of pwater, pice, and pcloud (not included) is 100" ;

probability_of_water:coordinates = "lon lat" ;

probability_of_water:valid_min = 0b ;

probability_of_water:valid_max = 100b ;

probability_of_water:_FillValue = -127b ;

byte probability_of_ice(time, nj, ni) ;

probability_of_ice:long_name = "probability of ice" ;

probability_of_ice:units = "percent" ;

probability_of_ice:comment = "Sum of pwater, pice, and pcloud (not included) is 100" ;

probability_of_ice:coordinates = "lon lat" ;

probability_of_ice:valid_min = 0b ;

probability_of_ice:valid_max = 100b ;

probability_of_ice:_FillValue = -127b ;

float wind_speed(time, nj, ni) ;

wind_speed:units = "m/s" ;

wind_speed:long_name = "10m wind speed" ;

wind_speed:standard_name = "wind_speed" ;

wind_speed:comment = "10m wind speed from ECMWF" ;

wind_speed:coordinates = "lon lat" ;

wind_speed:height = "10 m" ;

wind_speed:time_offset = 0s ;

wind_speed:valid_min = 0.f ;

wind_speed:valid_max = 100.f ;

wind_speed:_FillValue = -1.f ;

float t2m(time, nj, ni) ;

t2m:units = "K" ;

t2m:long_name = "air temperature, 2m" ;

t2m:standard_name = "air_temperature" ;

t2m:comment = "2m Temperature from ERA-INTERIM reanalysis, ECMWF" ;

t2m:coordinates = "lon lat" ;

t2m:valid_min = 150.f ;

t2m:valid_max = 350.f ;

t2m:_FillValue = -1.f ;

ubyte satellite_zenith_angle(time, nj, ni) ;

satellite_zenith_angle:long_name = "satellite zenith angle" ;

satellite_zenith_angle:units = "degree" ;

satellite_zenith_angle:comment = "Calculated satellite zenith angle based on the satellite geometry at the time of data acquisition" ;

satellite_zenith_angle:coordinates = "lon lat" ;

satellite_zenith_angle:valid_min = 0s ;

satellite_zenith_angle:valid_max = 80s ;

satellite_zenith_angle:_FillValue = 255UB ;

ubyte solar_zenith_angle(time, nj, ni) ;

solar_zenith_angle:units = "degrees" ;

solar_zenith_angle:long_name = "solar zenith angle" ;

solar_zenith_angle:valid_min = 0s ;

solar_zenith_angle:valid_max = 180s ;

solar_zenith_angle:coordinates = "lon lat" ;

solar_zenith_angle:_FillValue = 255UB ;

short large_scale_correlated_uncertainty(time, nj, ni) ;

large_scale_correlated_uncertainty:long_name = "Uncertainty from errors likely to be correlated over large scales" ;

large_scale_correlated_uncertainty:units = "K" ;

large_scale_correlated_uncertainty:coordinates = "lon lat" ;

large_scale_correlated_uncertainty:valid_min = 0s ;

large_scale_correlated_uncertainty:valid_max = 5000s ;

large_scale_correlated_uncertainty:scale_factor = 0.01f ;

large_scale_correlated_uncertainty:add_offset = 0.f ;

large_scale_correlated_uncertainty:comment = "Component of uncertainty that is correlated over large scales; can be combined with other uncertainty estimates to form a total uncertainty" ;

large_scale_correlated_uncertainty:_FillValue = -32768s ;

short uncorrelated_uncertainty(time, nj, ni) ;

uncorrelated_uncertainty:long_name = "Uncertainty from errors unlikely to be correlated between surface temperatures" ;

uncorrelated_uncertainty:units = "K" ;

uncorrelated_uncertainty:coordinates = "lon lat" ;

uncorrelated_uncertainty:valid_min = 0s ;

uncorrelated_uncertainty:valid_max = 5000s ;

uncorrelated_uncertainty:scale_factor = 0.01f ;

uncorrelated_uncertainty:add_offset = 0.f ;

uncorrelated_uncertainty:comment = "Component of uncertainty that is uncorrelated between SSTs; can be combined with other uncertainty estimates to form a total uncertainty" ;

uncorrelated_uncertainty:_FillValue = -32768s ;

short synoptically_correlated_uncertainty(time, nj, ni) ;

synoptically_correlated_uncertainty:long_name = "Uncertainty from errors likely to be correlated over synoptic scales" ;

synoptically_correlated_uncertainty:units = "K" ;

synoptically_correlated_uncertainty:coordinates = "lon lat" ;

synoptically_correlated_uncertainty:valid_min = 0s ;

synoptically_correlated_uncertainty:valid_max = 5000s ;

synoptically_correlated_uncertainty:scale_factor = 0.01f ;

synoptically_correlated_uncertainty:add_offset = 0.f ;

synoptically_correlated_uncertainty:comment = "Component of uncertainty that is correlated over synoptic scales; can be combined with other uncertainty estimates to form a total uncertainty" ;

synoptically_correlated_uncertainty:correlation_length_scale = "100 km" ;

synoptically_correlated_uncertainty:correlation_time_scale = "1 day" ;

synoptically_correlated_uncertainty:_FillValue = -32768s ;

// global attributes:

:topiccategory = "Oceans Climatology Meteorology Atmosphere" ;

:keywords = "Sea Ice Skin Temperature, Sea Surface Temperature, Sea Ice, Oceanography, Meteorology, Climate, Remote Sensing" ;

:gcmd_keywords = "Cryosphere > Sea Ice > Sea Ice Surface Temperature Ocean > Sea Surface > Sea Surface Temperature Geographic Region > Northern Hemipshere, above 60N Vertical Location > Sea SurfaceEUMETSAT OSISAF Greenland Climate and Research Center NORMAP" ;

:activity_type = "Space borne instrument" ;

:Conventions = "CF-1.6" ;

:spatial_resolution = "0.75 km at nadir" ;

:history = "2016-06-21 09:46:00 UTC creation" ;

:Metadata_Conventions = "Unidata Dataset Discovery v1.0" ;

:uuid = "b23e4b04-fa7d-48f8-bf0b-3157c322f5eb" ;

:source = "N/A" ;

:metadata_link = "N/A" ;

:keywords_vocabulary = "NASA Global Change Master Directory (GCMD) Science Keywords" ;

:standard_name_vocabulary = "NetCDF Climate and Forecast (CF) Metadata Convention" ;

:geospatial_lat_units = "degrees_north" ;

:geospatial_lat_resolution = 0.007f ;

:geospatial_lon_units = "degrees_east" ;

:geospatial_lon_resolution = 0.012f ;

:creator_name = "MET Norway" ;

:creator_email = "N/A" ;

:creator_url = "met.no" ;

:acknowledgment = "N/A" ;

:publisher_name = "N/A" ;

:publisher_url = "N/A" ;

:publisher_email = "N/A" ;

:processing_level = "L2P" ;

:cdm_data_type = "swath" ;

:date_created = "20160621T09:46:00Z" ;

:version = "v1.00" ;

:gds_version_id = "2.0" ;

:netcdf_version_id = "4.1.3" ;

:area = "North of 50N and South of 50S" ;

:PI_name = "Gorm Dybkjaer" ;

:contact = "gd@dmi.dk" ;

:license = "GHRSST protocol describes data use as free and open" ;

:project = "NACLIM(EU), NORMAP(N)" ;

:references = "Contact producer for documentation" ;

:title = "GAC reprocessing Level 2 - High Latitude Sea and Sea Ice Surface Temperature" ;

:summary = "Reprocessed Sea and Sea Ice Surface Temperature data set obtained from infrared satellite

imagery.The dataset is intended for data climate studies. Multible daily global swath products are freely available from the EUMETSAT data distributing system, EUMETCAST. This product is based on IR swath data, in from EUMETSAT Climate SAF N,from the NOAA satellite series since 1982. Data between latitude -40 and 40 are not processed and hence, only fill-values." ;

:product_name = "gac_ssist" ;

:id = "gac_ssist" ;

:product_status = "Beta version - with some empty fields containing no error statistics and probability fields." ;

:naming_authority = "org.ghrsst" ;

:institution = "Danish Meteorological Institute (dmi.dk) and Norwegian Meteorological Institute (MET)" ;

:satelliteID = "npp" ;

:date = "2016-06-21 08:16:00 UTC" ;

:start_time = "20160621T081643Z" ;

:stop_time = "20160621T083221Z" ;

:time_coverage_start = "20160621T081643Z" ;

:time_coverage_end = "20160621T083221Z" ;

:platform = "npp" ;

:sensor = "viirs" ;

:northernmost_latitude = 89.994f ;

:easternmost_longitude = 179.999f ;

:southernmost_latitude = 49.451f ;

:westernmost_longitude = -179.999f ;

:comment = "This product is based on IR swath data that are sensitive to atmospheric water. Hence, the swath data will contain areas with non valid surface temperature data." ;

7 References

Donlon, C.J., M. Martin, J. Stark, J. Roberts-Jones, E. Fiedler, W. Wimmer: The Operational Sea Surface Temperature and Sea Ice Analysis (OSTIA) system, Remote Sensing of Environment, Volume 116, 2012, Pages 140-158.

Dozier, J. and S.G. Warren: Effect of Viewing Angle on the Infrared BrightnessTemperature of Snow. WATER RESOURCES RESEARCH, 18, 5, pp. 1424-1434, 1982.

Dybbroe, A., A. Thoss and K.-G. Karlsson: NWC SAF AVHRR cloud detection and analysis using dynamic thresholds and radiative transfer modeling - Part I: Algorithm description, J. Appl. Meteor, 44, pp. 39-54, 2005a.

Dybbroe, A., A. Thoss and K.-G. Karlsson: NWC SAF AVHRR cloud detection and analysis using dynamic thresholds and radiative transfer modeling - Part II: Tuning and validation, J. Appl. Meteor, 44, 55-71, 2005b.

Dybbroe, A., Steinar Eastwood, Øystein Godøy, Ronald Scheirer and Mari Anne Killie: OSI-SAF/NWC-SAF Federated activity on cloud and ice masking in polar conditions – Evaluation report. OSI-SAF/NWC-SAF FEDERATED ACTIVITY.

DMI-TR 2011, Dybkjaer, G. (editor). The Qaanaaq sea ice thermal emission experiment - field report. DMI Technical Report 11-18. http://www.dmi.dk/fileadmin/ 2011.

Dybkjær, G., R. Tonboe, and J. L. Høyer: Arctic surface temperatures from Metop AVHRR compared to in situ ocean and land data. Ocean Sci., 8, 959–970, doi:10.5194/os-8-959-2012.

Dybkjær, G., J. Højer, R. Tonboe and S. Olsen. Report on the documentation and description of the new Arctic Ocean dataset combining SST and IST. NACLIM Deliverable D32.28. http://www.naclim.eu/ ; 2014.

Englyst, P., Høyer, J., Dybkjær, G., Tonboe, R. (2016). POSTER: Validation of Satellite Ice Surface Temperature Observations in the Arctic. Danish Meteorological Institute, Denmark. European Space Agency (ESA) Living Planet Symposium, Prague, Czech Republic.

ERAint. http://www.ecmwf.int/en/forecasts/datasets/era-interim-dataset-january-1979-present, 2014-09.

Fiduceo. Fidelity and uncertainty in climate data records from Earth Observations EU Horison 2020 project. http://www.fiduceo.eu ; 2016.

François C., A Brisson, P. Le Borgne, A. Marsouin: Definition of a radiosounding database for sea surface brightness temperature simulations: Application to sea surface temperature retrieval algorithm determination. Remote Sensing of Environment, 81, 2–3, pp 309–326, 2002.

GHRSST Science Team: The Recommended GHRSST Data Specification (GDS) 2.0, document revision 2, available from the GHRSST International Project Office, 2012.

Hall, D. K., J.R. Key, K.A. Casey, G.A. Riggs and D.J. Cavalieri: Sea Ice Surface

Temperature Product from MODIS, IEEE T. Geosci. Remote., 42, 1076–1087, 2004.

Hall, D. K., V. V. Salomonson, and G. A. Riggs. MODIS/Aqua Sea Ice Extent and IST Daily L3 Global 4km EASE-Grid Day. Version 5. Boulder, Colorado USA: National Snow and Ice Data Center. 2006.

Hocking, J. P. Rayer, D. Rundle, R. Saunders, M. Matricardi, A. Geer, P. Brunel and J. Vidot: RTTOV v11 User Guide, v1.3, 2014.

Jakobson et al. (2012), Validation of atmospheric reanalyses over the central Arctic Ocean, GRL, doi:10.1029/2012GL051591

Key, J. and M. Haefliger: Arctic Ice Surface Temperature Retrieval from AVHRR Thermal Channels, J. Geophys. Res.-Oc. Atm., 97, 5885–5893, 1992.

Key, J. R., Collins, J. B., Fowler, C., and Stone, R. S.: High-Latitude Surface Temperature Estimates from Thermal Satellite Data, Remote Sens. Environ., 61, 302–309, 1997.

Killie, M.A., Ø. Godøy, S. Eastwood and T. Lavergne: ATBD for the EUMETSAT OSI SAF Regional Ice Edge Product, v1.1, 2011.

Le Borgne, Pierre, S.Péré and H. Roquet. METOP-A/AVHRR derived SST over the Arctic 6 years (2007-2012) daytime results. Working Paper, Météo-France, CMS, 2014.

Lupkes et al. (2010),Meteorological observations from ship cruises during summer to the central Arctic: A comparison with reanalysis data, GRL, doi:10.1029/2010GL042724.

Mittaz, Jonathan. Dept. of Meteorology, University of ReadingRoom 284b, Harry Pitt Building, 3 Earley Gate, PO Box 238 Whiteknights, Reading, RG6 6AL. Personal communication.

NOAAngdc. National Oceanic and Atmospheric Administration, National Geophysical Data Centre. http://www.ngdc.noaa.gov/mgg/global/global.html, 2014-09

NWCSAF. http://www.nwcsaf.org, 2014-09.

OSI SAF project team: Low earth orbiter sea surface temperature product user manual. Version 2.6. Prepared by Météo France, 2014.

PPScloud. The Polar Platform System package, Product User Manual for "Cloud Products". http://www.nwcsaf.org/HD/MainNS.jsp, CMa-PGE01 v3.2, CT-PGE02 v2.2 & CTTH-PGE03 v2.2, 2014-09

PRD. OSI SAF CDOP 3 Product Requirement Document, v1.1, 2017. http://www.osi-saf.org/?q=content/product-requirement-document-3

Saux Picart, S.: ATBD for the LEO SST Processing Chain (OSI-201b, OSI-202b, OSI-204b), v1.0 (2014).

Stammer, D., Johanessen, J., LeTraon, P.-Y., Minnett, P., Roquet,H., and Srokosz, M.: Requirements for Ocean Observations Rel-evant to post-EPS, EUMETSAT Position Paper: AEG Ocean To-pography and Ocean Imaging, 10 January 2007, version 3, 2007.

Vincent, R. F., R. F. Marsden, P. J.Minnett, K. A.M. Creber and J.R. Buckley: Arctic waters and marginal ice zones: A composite Arctic sea surface temperature algorithm using satellite thermal data, J. Geophys. Res.-Oceans, 113, C04021, doi:10.1029/2007JC004353, 2008.